Mimicking Co-Transcriptional RNA Folding Using a Superhelicase

Boyang Hua[†,‡], Subrata Panja[#,‡], Yanbo Wang[†], Sarah A. Woodson[*,#] and Taekjip Ha[*,†,#,^,§]

[†]Department of Biophysics and Biophysical Chemistry, Johns Hopkins School of Medicine, Baltimore, Maryland 21205, United States

[#]T. C. Jenkins Department of Biophysics, Johns Hopkins University, Baltimore, Maryland 21218, United States

[^]Department of Biomedical Engineering, Johns Hopkins University, Baltimore, Maryland 21218, United States

[§]Howard Hughes Medical Institute, Baltimore, Maryland 21205, United States

[‡]These authors contributed equally.

[*]Email(s): swoodson@jhu.edu (S. A. W.) and tjha@jhu.edu (T. H.)

METHODS

RNA preparation

For this study we used the 54 nt *Osa* 1–4 unimolecular twister ribozyme from *O. sativa*.[S1, 20] Fluorophore-labeled twister RNA was prepared by splint free ligation of two fragments with T4 RNA ligase I as described in ref. S2. The ligated product was gel purified and buffer exchanged as described in ref. 20. Synthetic RNA fragments for ligation were purchased from IDT in a reverse phase HPLC purified form; DNA oligomers were purchased from IDT without HPLC purification.

For the vectorial folding and refolding assays, we used the 5' fragment that contains a Cy3 fluorophore in the backbone of the RNA between rG23 and rU24 (IDT Int Cy3):

5'-rCCGCCdUrAACACUGCCAAUGCCGG-(Cy3)-UCCCA-3'.

To observe the maiden 2D folding, we used another 5' fragment that contains a Cy3 fluorophore at the 5'-end of the RNA:

5'-(Cy3)-rCCGCCdUrAACACUGCCAAUGCCGGUCCCA-3'.

In both constructs, U6 was replaced with dU6 to prevent phosphodiester bond cleavage.

The 3' fragment of *Osa* twister ribozyme was extended with deoxyribonucleotides to hybridize with a Cy5-labeled anchor DNA:

5'-r(AGCCCGGAUAAAAGUGGAGGGGGCGG)d(AGGACGACACACTTTGGACAGGACACACAGGACACAGG)-3'.

The anchor DNA (Bio-SA5-Cy5):

5'-(biotin)-dCCTGTGTCCTGTGTGTCCTGTCCAAAGTGTGTCGTCC-(Cy5)-3'.

For vectorial folding assays, we used a single-stranded DNA complementary to the twister RNA with a dT_{20} 3' overhang to facilitate Rep-X binding (OstCD):

5'-GCCCCCTCCACTTTTATCCGGGCTTGGGACCGGCATTGGCAGTGTTAGGCGGTTTTTTTTTTTTTTTTTT-3'.

Sample preparation for the single-molecule FRET measurements

For vectorial folding assays, 40 nM twister RNA was annealed with 20 nM Bio-SA5-Cy5 and 80 nM OstCD in 10 µl of 1× HK buffer [30 mM K-HEPES (pH 7.5) and 100 mM KCl] by incubating the mixture at 95 °C for 1 min, 75 °C for 5 min, 37 °C for 15 min and finally equilibrating at room temperature for 5 min. For refolding assays, sample preparation was the same as described above, except that OstCD was not added to the annealing complex.

The vectorial folding assay (VFA)

Labeled and biotinylated heteroduplexes were immobilized on a neutravidin-functionalized surface and free heteroduplexes were washed out. Rep-X was incubated with heteroduplexes in the loading buffer for 2 min. Unless specified otherwise, the loading buffer contained 20 nM Rep-X, 30 mM K-HEPES (pH 7.5), 2 % glycerol and no added KCl (< 3 mM). Free Rep-X was washed out and unwinding was initiated by adding the unwinding buffer. Unless specified otherwise, the unwinding buffer contained 30 mM K-HEPES (pH 7.5), 20 mM $MgCl_2$, 1 mM ATP, and 2 % glycerol. In some experiments, we also included a trap DNA strand in the unwinding buffer (100 nM). The trap DNA is complementary to the cDNA so that it will trap the released cDNA and prevent the cDNA from reannealing to the twister strand. However, we did not observe a difference in the unwinding yields between VFA done with and without the trap DNA (data not shown). For characterization of VFA products at equilibrium, images were taken 5 min after the addition of the unwinding buffer. For the real-time observation ("flow-in" experiments), imaging was started a few seconds before the addition of the unwinding buffer. The loading and unwinding buffers used during imaging contained additional 4 mM Trolox, 0.8 % wt/vol glucose, 165 U/ml glucose oxidase and 2170 U/ml catalase to reduce the photobleaching rate.[S3]

Multiple-turnover VFA were performed by incubating the heteroduplexes with 50 nM Rep-X, 10 mM ATP and 20 mM $MgCl_2$ for > 5 min to enable multiple rounds of unwinding by Rep-X. This multiple turnover assay (with respect to Rep-X) yielded 96 % normalized unwinding.

When PcrA-X was used in place of Rep-X, 100 nM of PcrA-X was added in the loading buffer and 0.2 mM ATP was used in the unwinding buffer. Other buffer components were kept the same.

The refolding assay (RFA)

Labeled and biotinylated twister molecules (without cDNA) were immobilized on a neutravidin-functionalized surface and free twister molecules were washed out. 2D structures of the twister RNA were fully equilibrated in the buffer containing 30 mM K-HEPES (pH 7.5), 2 % glycerol and no added KCl (< 3 mM). Refolding was initiated by adding the refolding buffer. Unless specified otherwise, the refolding buffer contained 30 mM K-HEPES (pH 7.5), 20 mM $MgCl_2$, and 2 % glycerol. For characterization of RFA products at equilibrium, images were taken 5 min after the addition of the refolding buffer. For the real-time observation ("flow-in" experiments), imaging was started a few seconds before the addition of the refolding buffer. The refolding buffers used during imaging contained additional 4 mM Trolox, 0.8 % wt/vol glucose, 165 U/ml glucose oxidase and 2170 U/ml catalase to reduce the photobleaching rate.[S3]

The single-molecule imaging system

The single-molecule imaging system was adapted from ref. S4 with minor modification. We imaged flow chamber under a prism-based total internal reflection fluorescence (TIRF) imaging microscope.[S5] A 532-nm laser (Coherent Compass 315M) and

a 633-nm laser (Cobolt 06-MLD) were used for Cy3 and Cy5 excitation, respectively. The fluorescence emission was collected by a water immersion objective (Olympus NA 1.2, 60 ×) and recorded by an EMCCD camera (Andor Technology IXon 897) with 0.05 s time resolution. The fluorescence emission filters used were a long-pass filter (Semrock BLP02-561R-25) for rejecting the 532-nm laser and a notch filter (Chroma ZET633TopNotch) for rejecting the 633-nm laser. A long-pass dichroic mirror (Semrock FF640-FDi01-25x36) was used to separate the donor and acceptor emission.

The PEG surfaces were prepared and used according to ref. S6. The DT20 surfaces were prepared and used according to ref. S7.

Single-molecule data analysis

Single-molecule spots were detected and further analyzed by custom codes. Background subtraction, donor leakage and acceptor direct-excitation correction were performed according to ref. S8. All custom codes are available upon request.

We determined the center of PIFE peak in each "flow-in" trajectory with Gaussian fitting (Figure S3). To estimate the ATP injection time of each movie, we calculated the average time of PIFE peak centers within each movie. We then aligned the time frames of different movies accordingly, so that the unwinding and folding kinetics of molecules in different movies could be compared.

Determination of the normalized unwinding yield of VFA

Using the criterion of forming 3D structures (native or non-native) at least once before the end of the observation, we determined the percentage of the twister molecules (29 %) that were released from the cDNA. However, this criterion may underestimate the extent of unwinding, since some unwound molecules could fail to show a mid-to-high FRET signal due to chemical heterogeneity, surface immobilization and limited observation time window before photobleaching. To account for these effects, we normalized the unwinding yield in VFA to the fraction of molecules that were able to form 3D structures at least once in RFA at the same $MgCl_2$ concentration (83 % at 20 mM $MgCl_2$).

Simulation of the co-transcriptional folding pathway of twister

To simulate the co-transcriptional folding pathway of twister, we started with the first 10 nt at the 5'-end of the *Osa* 1–4 unimolecular twister ribozyme construct. Then we generated a library of twister sequences by adding one nucleotide at a time to the 3'-end of the initial sequence. Then we determined the 2D structure of each sequence by 'Vienna RNAfold Web Server'[S9] and 'RNAstructure Web Server'[S10]. From the ensemble of structures, we selected the minimum energy structure. The 2D structure progression was validated by another RNA structure predicting software 'KineFold Web Server'[S11].

SUPPLEMENTARY FIGURES

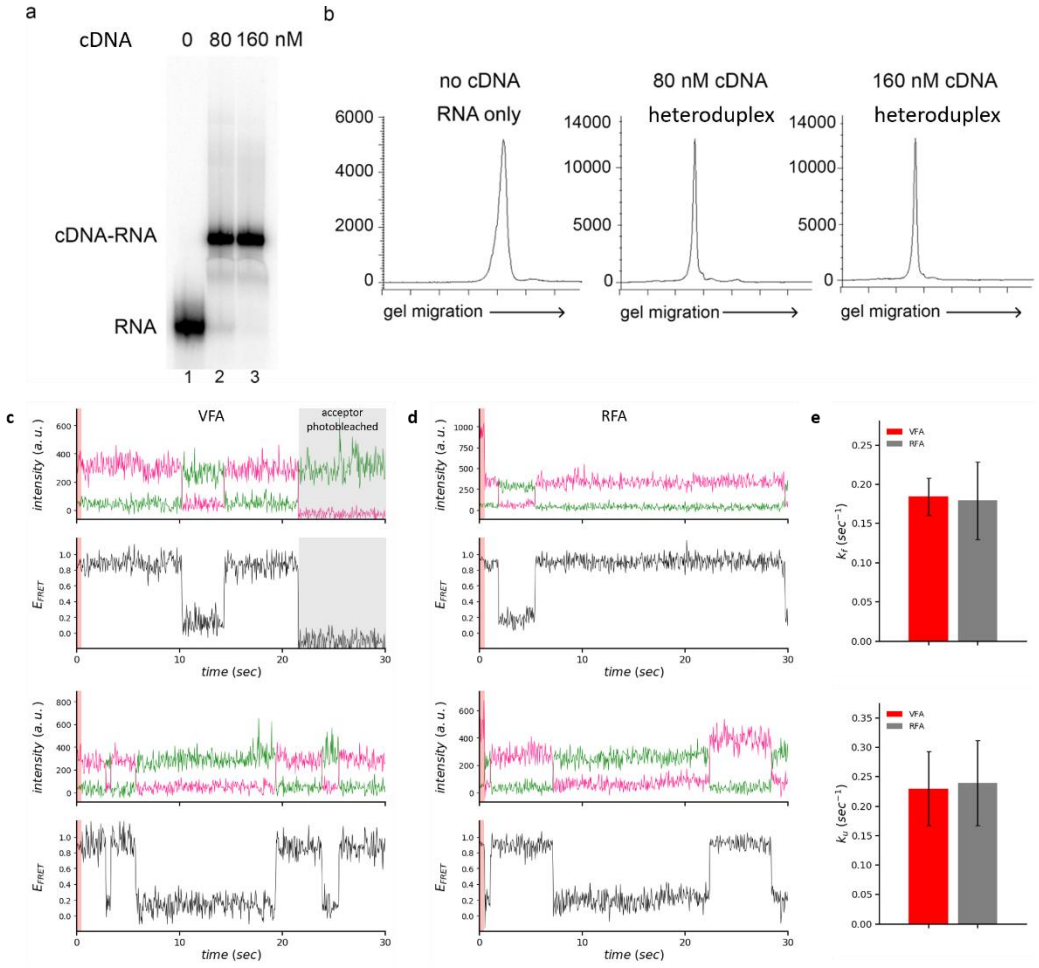

Figure S1. Twister ribozyme folding after heteroduplex unwinding. (**a-b**) In order to determine the annealing efficiency of the cDNA–*Osa* twister RNA heteroduplex, the heteroduplex was prepared as for single-molecule FRET experiments and analyzed by native PAGE. 5 nM ^{32}P-*Osa* twister RNA and 35 nM unlabeled *Osa* twister RNA were mixed with 80 or 160 nM cDNA in 1× HK buffer (10 µl total volume). Sample mixtures were incubated at 95 °C for 1 min, 75 °C for 5 min and 37 °C for 15 min in a thermocycler, and then held at room temperature for 5 min before being loaded in a nondenaturing 6 % polyacrylamide gel. cDNA–RNA heteroduplexes were separated from the free RNA by running the samples at 10 watts for 1 hour in 1× TBE. (**a**) Image of the gel showing cDNA–RNA heteroduplexes. (**b**) Intensity of the bands as a function of migration distance for each lane of the gel. cDNA–RNA heteroduplexes (lanes 2 & 3) migrated slower and had a narrower distribution of band intensity than the RNA (lane 1), suggesting that the heteroduplex is more conformationally homogeneous than the RNA itself. (**c-d**) FRET trajectories of twister molecules at equilibrium after VFA (**c**) and RFA (**d**). Regions highlighted in red indicate sample illumination with the 633-nm laser to confirm the presence of the acceptor (Cy5) fluorophore. (**e**) The folding and unfolding rates of twister molecules at equilibrium from VFA and RFA. To determine the rates, ($k_f + k_u$) was calculated by the cross-correlation analysis of donor and acceptor intensities and (k_f / k_u) by the population ratio from FRET histograms. The error bars represent s.e.m. (n = 3). Each repeat used 20–60 FRET trajectories. The $MgCl_2$ concentration used in this figure was 20 mM.

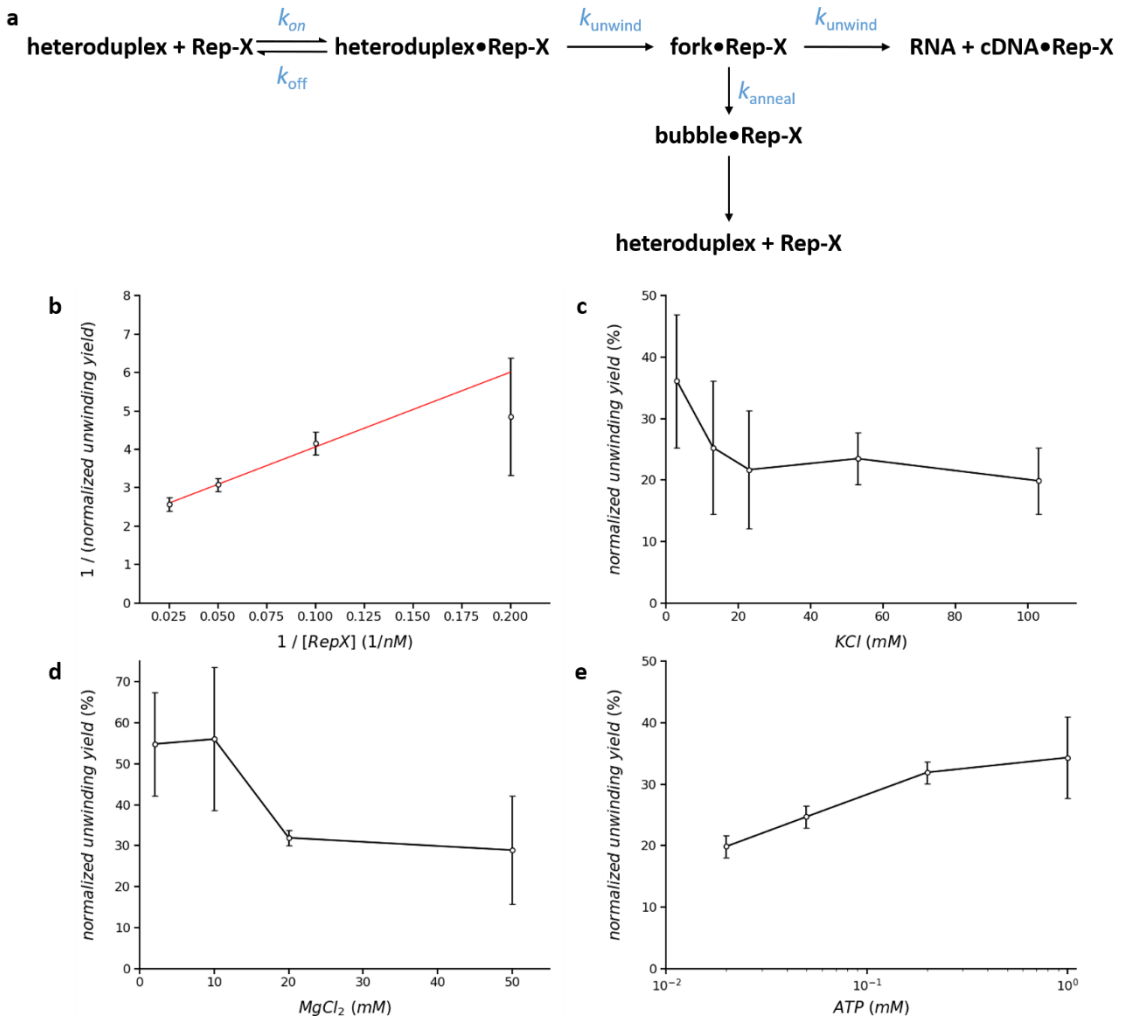

Figure S2. Characterization of the unwinding yields in VFA. (**a**) Kinetic model for Rep-X unwinding in VFA. In a simple model for helicase unwinding yield, the yield is determined by the fraction of heteroduplexes bound by Rep-X in the helicase loading step and the efficiency of RNA release by Rep-X in a single-turnover unwinding reaction. Possible reasons for unsuccessful RNA release include Rep-X dissociation before unwinding starts and DNA–RNA reannealing after Rep-X goes through. (**b**) Titration of the Rep-X concentration in the helicase loading step. The error bars represent the standard deviation (n = 2–3). The red line is a linear fit with instrumental weighting on errors. We determined the dissociation constant between the heteroduplex and Rep-X to be 9.2 nM and the efficiency of RNA release to be 0.47. (**c**-**e**) Titration of Rep-X•heteroduplex complexes with KCl (c), $MgCl_2$ (d) and ATP (e) in the unwinding step. The error bars represent s.e.m. (n = 2). The unwinding yields were determined by counting individual doubly labeled molecules. The normalized unwinding yield decreased to about 20 % at the highest salt concentrations tested (100 mM KCl and 50 mM $MgCl_2$, respectively). The observed effect of salt concentrations on the unwinding yield largely depends on the ionic strength and is not ion type-specific; thus, it can be explained by the accelerated Rep-X dissociation caused by stronger charge screening at elevated salt concentrations.[21] At 20 mM $MgCl_2$, the unwinding yield was unaffected by lowering the ATP concentration from 1 mM to 0.2 mM but was reduced by further lowering the ATP concentration below 50 μM. Overall, these results demonstrate that the superhelicase-based VFA works at a wide range of salt and ATP concentrations.

We chose 20 nM Rep-X and no added KCl (< 3 mM) as the standard loading condition and 20 mM $MgCl_2$, 1 mM ATP and no added KCl as the standard unwinding condition (Methods).

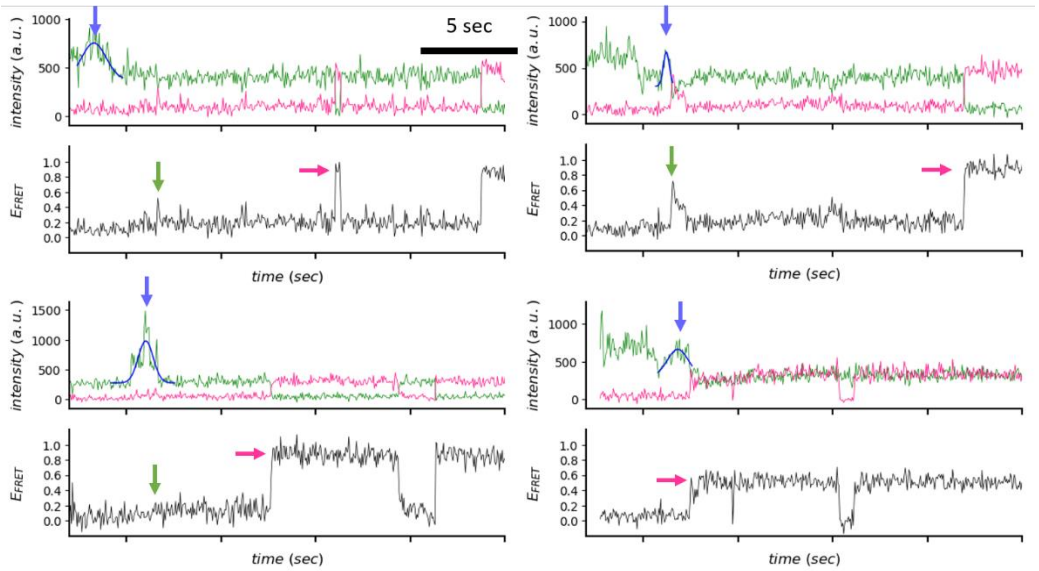

Figure S3. Examples of VFA trajectories using Rep-X. FRET trajectories showing the PIFE peaks (blue arrow) and the maiden 2D (green arrow) and 3D (magenta arrow) folding events. The center of each PIFE peak was determined by Gaussian fitting.

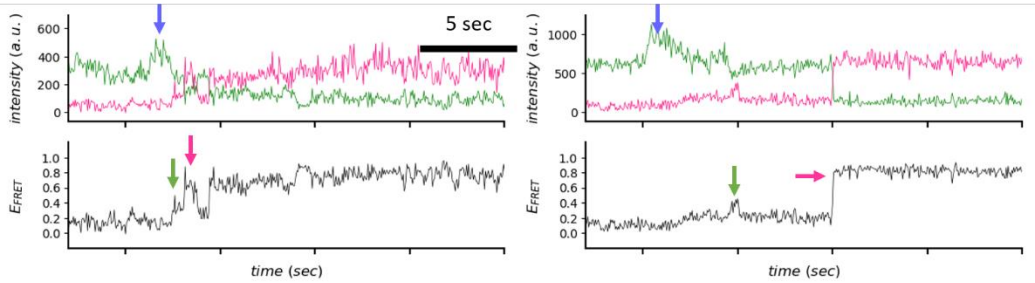

Figure S4. Examples of VFA trajectories using PcrA-X helicase. FRET trajectories showing the PIFE peaks (blue arrow) and the maiden 2D (green arrow) and 3D (magenta arrow) folding events.

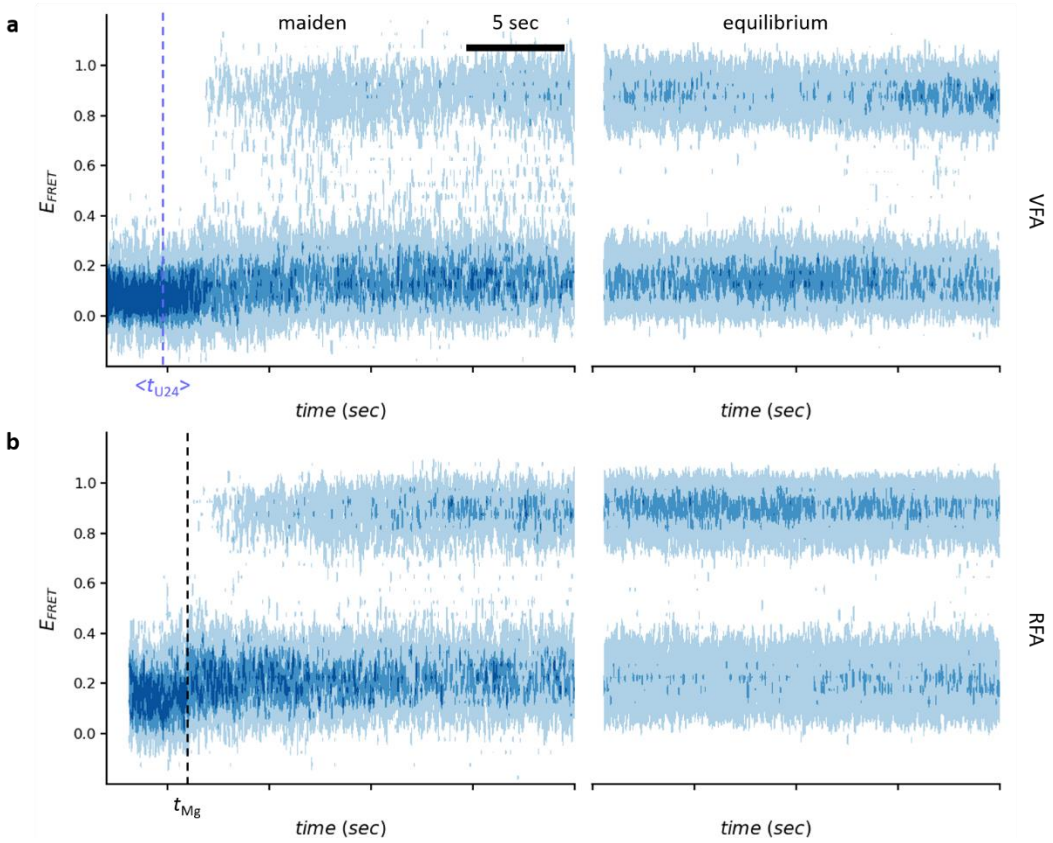

Figure S5. 2D FRET histograms built from all the trajectories from the "flow-in" experiments. (**a**) VFA in the maiden phase (left) and at equilibrium (right). (**b**) RFA in the maiden phase (left) and at equilibrium (right).

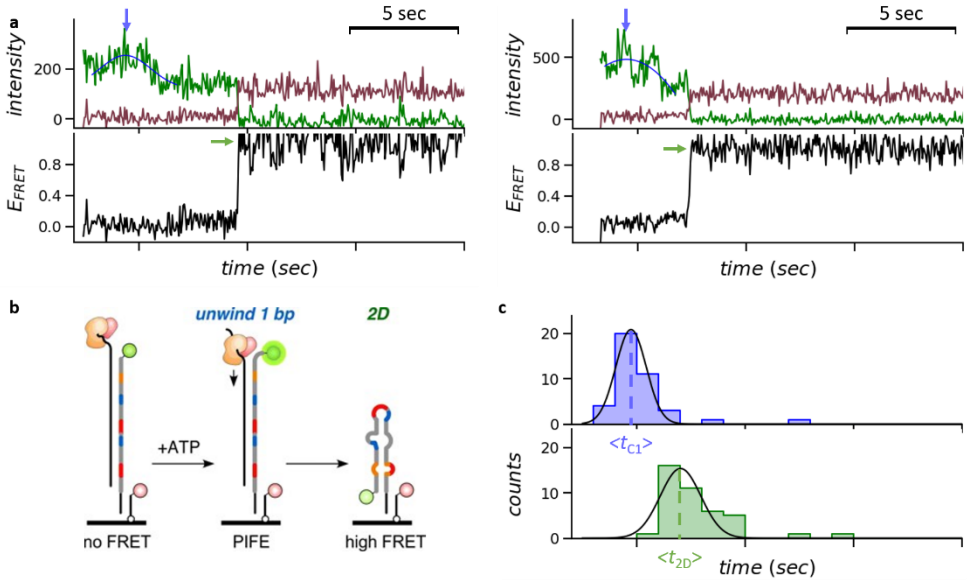

Figure S6. Real-time observation of the unwinding and folding signals in VFA on twister ribozyme with the Cy3 fluorophore attached at C1. (**a**) FRET trajectories showing the PIFE peaks (blue arrow) and the maiden 2D (green arrow) folding events. The center of each PIFE peak was determined by Gaussian fitting. (**b**) Schematics of the "order-of-events" in VFA. (**c**) Time histograms of the PIFE peak centers and the maiden 2D folding transitions, respectively. Gaussian fitting determined the average times (as marked by the dotted lines). The Δt_{2D-C1} was 2.3 s.

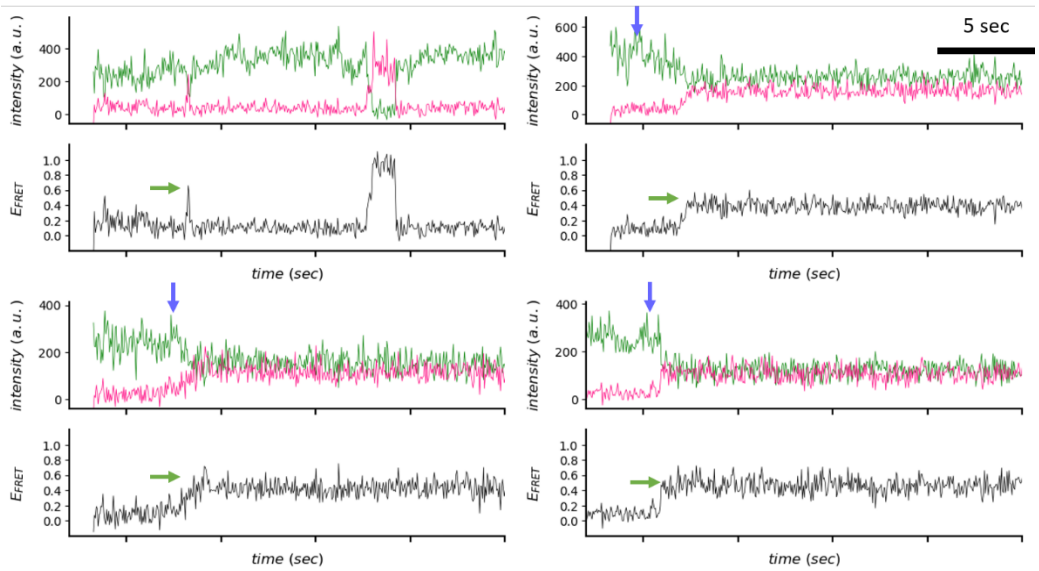

Figure S7. Examples of VFA trajectories of twister ribozyme with the Cy3 fluorophore attached at C1 showed maiden 2D misfolding. FRET trajectories showing the PIFE peaks (blue arrow) and the maiden 2D (green arrow) folding events.

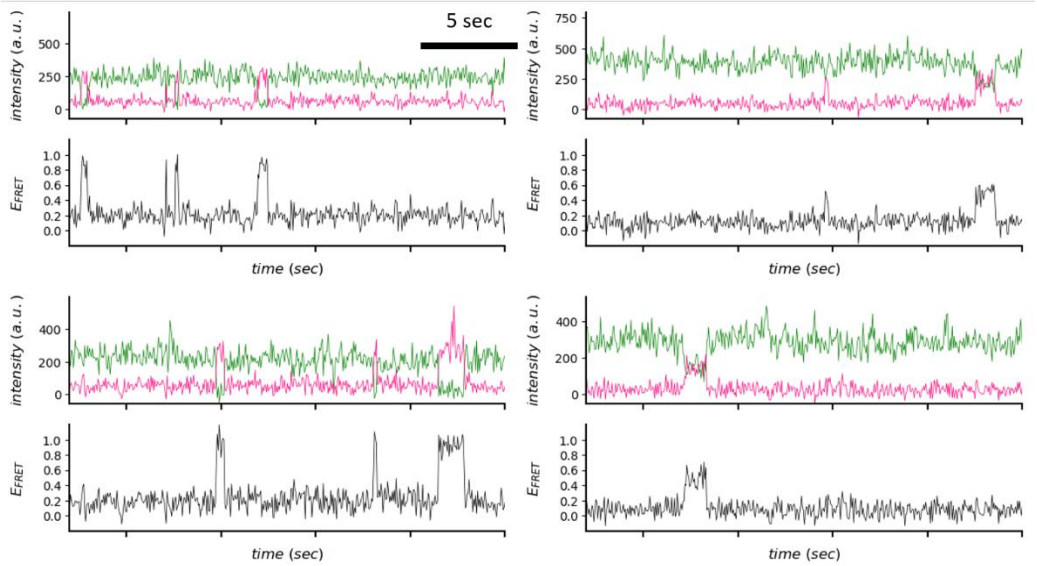

Figure S8. Examples of RFA trajectories of the G48A mutant at equilibrium at 20 mM $MgCl_2$.

References

(S1) Liu, Y., Wilson, T. J., McPhee, S. A., Lilley, D. M. (2014) *Nat. Chem. Biol.* 10, 739–744.

(S2) Solomatin, S., Herschlag, D. (2009) *Methods Enzymol.* 469, 47–68.

(S3) Rasnik, I., McKinney, S. A., Ha, T. (2006) *Nat. Methods* 3, 891–893.

(S4) Hua, B., Wang. Y., Park, S., Han, K. Y., Singh, D., Kim, J. H., Cheng, W., Ha, T. (2018) *Biochemistry* 57, 1572–1576.

(S5) Joo, C., Ha, T. (2007) *Single molecule techniques: A Laboratory Manual* Selvin, P., Ha, T. editors. Cold Spring Harbor Laboratory Press, Cold Spring Harbor, NY ch. 2, p. 3–36.

(S6) Ha, T., Rasnik, I., Cheng, W., Babcock, H. P., Gauss, G. H., Lohman, T. M., Chu, S. (2002) *Nature* 419, 638–641.

(S7) Hua, B., Han, K. Y., Zhou, R., Kim, H., Shi, X., Abeysirigunawardena, S. C., Jain, A., Singh, D., Aggarwal, V., Woodson, S. A., Ha, T. (2014) *Nat. Methods* 11, 1233−1236.

(S8) Margeat, E., Kapanidis, A. N., Tinnefeld, P., Wang, Y., Mukhopadhyay, J., Ebright, R. H., Weiss, S. (2006) *Biophys. J.* 90, 1419–1431.

(S9) Gruber, A. R., Lorenz, R., Bernhart, S. H., Neuböck, R., Hofacker, I. L. (2008) *Nucleic Acids Res.* 36, W70–W74.

(S10) Bellaousov, S., Reuter, J. S., Seetin, M. G., Mathews, D. H. (2013). *Nucleic Acids Res.* 41, W471–W474.

(S11) Xayaphoummine, A., Bucher, T., Isambert, H. (2005) *Nucleic Acids Res.* 33, W605–W610.